Radiative capture and electromagnetic dissociation involving loosely bound nuclei: The ^{8}B example

C. Forssén,* N. B. Shul'gina,† and M. V. Zhukov

Chalmers University of Technology and Göteborg University, S–412 96 Göteborg, Sweden

(Received 21 January 2003; published 28 April 2003)

Electromagnetic processes in loosely bound nuclei are investigated using an analytical model. In particular, electromagnetic dissociation of ^{8}B is studied and the results of our analytical model are compared to numerical calculations based on a three-body picture of the ^{8}B bound state. The calculation of energy spectra is shown to be strongly model dependent. This is demonstrated by investigating the sensitivity to the rms intercluster distance, the few-body behavior, and the effects of final state interaction. In contrast, the fraction of the energy spectrum which can be attributed to $E1$ transitions is found to be almost model independent at small relative energies. This finding is of great importance for astrophysical applications as it provides us with a new tool to extract the $E1$ component from measured energy spectra. An additional, and independent, method is also proposed as it is demonstrated how two sets of experimental data, obtained with different beam energy and/or minimum impact parameter, can be used to extract the $E1$ component.

I. INTRODUCTION

The properties of loosely bound nuclei have been studied in nuclear physics for a number of years. In particular some electromagnetic processes, such as certain charged particle capture reactions, are very interesting in themselves as they are of vital importance in astrophysical scenarios. Unfortunately, at stellar energies, the cross sections for these reactions are very small due to the Coulomb barrier and direct measurements are therefore extremely difficult. Instead one has to rely on theoretical extrapolations from experimentally accessible energies down to stellar ones. An alternative, indirect method to investigate radiative capture reactions, is to study electromagnetic dissociation (EMD) on heavy targets [1]. This technique gives an enormous increase in yield due to the huge amount of virtual photons produced by the high-Z target, the more favorable phase space factor, and the possibility to use thicker targets. In principle, it should therefore be possible to measure the cross section at very low relative energies. There are, however, also disadvantages with the indirect method; the most important being the admixture of γ transitions with different multipolarities whereas the direct capture process, in most cases, should be completely dominated by $E1$ transitions. Since the cross sections for radiative capture and photodissociation are related via detailed balance for each separate multipole, it is necessary to have knowledge of the strengths of different multipole transitions in the EMD reaction.

The problem of extracting the $E1$ contribution from a measured EMD energy spectrum remains a challenge to the nuclear physics community. In Ref. [2], it was proposed to study the angular or momentum distributions of the breakup fragments. The idea was to employ the fact that interference terms, between $E1$ and $E2$ excitation amplitudes, will produce an asymmetry in these distributions. This method was, e.g., used in the analysis of ^{8}B EMD [3] where the $E2$ excitation amplitude, calculated within first-order perturbation theory, was renormalized in order to reproduce the asymmetry of the measured ^{7}Be longitudinal momentum distribution. However, as was already noted in Ref. [2], the asymmetry due to $E1$-$E2$ interference strongly depends on the final state interaction (FSI) between the breakup fragments; or in other words, on the structure of the continuum up to relatively large energies. Moreover, terms which contribute to the asymmetry do not contribute to the integrated cross section from which the astrophysical S factor is extracted. Finally, for low beam energies, higher-order dynamical effects will lead to a reduction of the asymmetry [4]. Therefore we conclude that, if we are interested in astrophysical applications of EMD experiments, it is desirable to look for more stable, and less model dependent, characteristics than the asymmetries of angular and momentum distributions. In this paper, we will present two novel methods to extract the $E1/E2$ ratio from EMD experiments.

We will use an analytical approach based on a two-cluster picture of the nucleus, but the effects of many-body structure will also be included. Our approach will be general in the sense that both neutron-rich and proton-rich systems can be studied. This model was first presented in Ref. [5] while similar approaches also exist for one-neutron [6,7] and two-neutron [8–10] halo nuclei. Although advanced numerical investigations are readily performed utilizing present day computer power, an analytical approach might have an advantage when exploring general physics features, and the sensitivity to different model assumptions.

The physics case which will be investigated throughout this paper is the ^{8}B nucleus. The interest in ^{8}B stems from its key role in the production of high-energy solar neutrinos. It is well known that the probability for the reaction ^{7}Be$(p,\gamma)^8$B at solar energies strongly depends on the structure of ^{8}B and, in particular, on the asymptotics of the va-

*Electronic address: c.forssen@fy.chalmers.se

†Permanent address: The Kurchatov Institute, RU-123182 Moscow, Russia.

lence proton wave function (WF). This reaction has been studied indirectly through EMD, using a radioactive ^{8}B beam impinging on a heavy target [3,11–13]. Note that the question of $E2$ contributions to the experimental spectra was addressed differently in all these investigations. We should also mention the recent progress in radiative capture measurements [14], where the cross section has been measured at energies around 200 keV with an accuracy of $\approx 15\%$. Nevertheless, in all cases theoretical models are needed to extrapolate the measured cross sections down to solar energies. Theoretical studies of the low-energy behavior of the astrophysical S_{17} factor have been presented by many authors, see, e.g., Refs. [15–21].

The structure of this paper is the following: Section II contains a summary of the theoretical framework that will be used in the calculations. In Sec. III our analytical model WFs are presented and discussed in quite some detail. Finally, in Sec. IV we discuss the model dependence of calculated EMD energy spectra and propose two new methods to extract information from EMD experiments.

II. THEORETICAL FRAMEWORK

Our starting point for calculating electromagnetic cross sections will be the Eλ strength function for a transition from a bound state (total spin J_0) to a continuum state with energy E

$$\frac{dB(\mathrm{E}\lambda)}{dE} = \frac{1}{2J_0+1} \sum_j \int d\tau_j |\langle j||\mathcal{M}(\mathrm{E}\lambda)||0\rangle|^2 \delta(E_j-E), \tag{1}$$

where $d\tau_j$ is the phase space element for final states, $\mathcal{M}(\mathrm{E}\lambda,\mu)$ is the electric multipole operator, and $|0\rangle$, $|j\rangle$ are the bound and continuum states in the center of mass system.

We will consider loosely bound systems of two clusters $(c+x)$ and, in particular, we will study transitions to the low-energy continuum in which excitations are manifested as relative motion between the clusters $E=\hbar^2 k^2/2\mu_{cx}$, where μ_{cx} is the reduced mass of the two-body system. Introducing the intercluster distance r, the corresponding cluster Eλ operator (operating only on the relative motion of clusters) is

$$\mathcal{M}(\mathrm{E}\lambda,\mu) = eZ(\lambda)r^\lambda Y_{\lambda\mu}(\hat{r}), \tag{2}$$

where we have also introduced the effective multipole charge $Z(\lambda) = \mu_{cx}^\lambda [Z_x/m_x^\lambda + (-1)^\lambda Z_c/m_c^\lambda]$.

The strength function is the key to study several reactions. For example, the cross section for photodissociation $A(\gamma,x)c$ is given by

$$\sigma_\gamma^{\mathrm{E}\lambda}(E) = \frac{(2\pi)^3(\lambda+1)}{\lambda[(2\lambda+1)!!]^2} \left(\frac{E_\gamma}{\hbar c}\right)^{2\lambda-1} \frac{dB(\mathrm{E}\lambda)}{dE}, \tag{3}$$

where the photon energy $E_\gamma = E + E_0$ is larger than the binding energy E_0. From this formula the inverse radiative capture reaction $c(x,\gamma)A$ can be studied using detailed balance

$$\sigma_{\mathrm{rc}}^{\mathrm{E}\lambda}(E) = \left(\frac{E_\gamma}{\hbar c k}\right)^2 \frac{2(2J_A+1)}{(2J_c+1)(2J_x+1)} \sigma_\gamma^{\mathrm{E}\lambda}(E), \tag{4}$$

where J_i is the spin of particle i. Note that the probability for direct capture of charged particles is dramatically reduced at low energies due to the Coulomb barrier in the $c+x$ channel. The cross section is therefore usually factorized into the Gamow penetration factor and the S factor

$$\sigma_{\mathrm{rc}}(E) = \frac{e^{-2\pi\eta(k)}}{E} S(E), \tag{5}$$

where $\eta(k) = Z_c Z_x e^2 \mu_{cx}/\hbar^2 k$ is the Sommerfeld parameter. The dominant part of the energy behavior is carried by the Gamow penetration factor while, e.g., nuclear structure information is incorporated into the S factor.

Finally, we will consider the process of EMD on a high-Z target. Using first-order perturbation theory, and the method of virtual quanta [22,23], the energy spectrum can be written as a sum over multipole $(\pi\lambda)$ photodissociation cross sections multiplied by the corresponding spectra of virtual photons $n_{\pi\lambda}(E_\gamma)$,

$$\frac{d\sigma_{\mathrm{EMD}}}{dE} = \sum_{\mathrm{E}\lambda} \frac{n_{\mathrm{E}\lambda}(E_\gamma)}{E_\gamma} \sigma_\gamma^{\mathrm{E}\lambda}(E) + \sum_{\mathrm{M}\lambda} \frac{n_{\mathrm{M}\lambda}(E_\gamma)}{E_\gamma} \sigma_\gamma^{\mathrm{M}\lambda}(E). \tag{6}$$

Note that, except in the vicinity of corresponding resonances, Mλ transitions are usually strongly suppressed [23]. Therefore, we will not study them in this work.

III. ANALYTICAL MODEL

A. Model wave functions

A straightforward calculation of the electric multipole matrix element for a direct transition between a loosely bound state and a nonresonant continuum state shows that the radial integrand rises to a maximum value at a radius which is, in most cases, many times the nuclear radius. Thus, these processes will mainly probe the surface structure of the nucleus. Furthermore, "loosely bound" implies that the nucleus will exhibit a large degree of clusterization and that the relative motion WF between the core and the valence nucleon will have an extended tail.

The final, continuum state will contain both Coulomb and nuclear distortions. For low continuum energies, and when the binding energy of the initial state is small, the nuclear distortions can be neglected in a first approximation. Therefore, we will only consider a pure Coulomb continuum in our analytical model, i.e., all nuclear phase shifts will be put equal to zero. The effects of nuclear distortions in ^{8}B EMD will be considered in Sec. IV A. Thus, a continuum state, with relative orbital momentum l between the clusters, will be described by a normalized, regular Coulomb function

$$\phi_l(k,r) = \sqrt{\frac{2}{\pi}} \frac{1}{k} i^l e^{i\sigma_l} F_l(k,r), \tag{7}$$

where

$$F_l(k,r) = C_l(k)e^{ikr}(kr)^{l+1} {}_1F_1$$
$$\times (l+1+i\eta(k);2l+2;-2ikr), \quad (8)$$

and σ_l is the Coulomb phase, $\eta(k)$ is the Sommerfeld parameter, ${}_1F_1(a;b;z)$ is the confluent hypergeometric function [24], and

$$C_l(k) = 2^l e^{-\pi\eta(k)/2} |\Gamma(l+1+i\eta(k))|/(2l+1)!. \quad (9)$$

The reduced matrix element introduced in the definition of the strength function, Eq. (1), contains a radial integral. With our approximation for the continuum state this integral takes the form

$$I_l(k) = \int_0^\infty dr \, e^{-ikr} r^{l+1} {}_1F_1$$
$$\times (l+1-i\eta(k);2l+2;2ikr) r^\lambda \phi(0,r). \quad (10)$$

Here, $\phi(0,r)$ is the two-body, relative motion WF describing the initial, bound state. At large r, with relative orbital momentum l_0 between the clusters, this radial function should be proportional to the Whittaker function $W_{-\eta_0, l_0+1/2}(2\kappa_0 r)$, see, e.g., Ref. [24], where $\eta_0 = Z_c Z_x e^2 \mu_{cx}/\hbar^2 \kappa_0$ and $E_0 = \hbar^2 \kappa_0^2/2\mu_{cx}$ is the binding energy.

In most studies on loosely bound systems, the Whittaker function has been used to describe the bound state for all r. However, the Whittaker function behaves as r^{-l_0} in the limit $r \to 0$, and therefore this approximation is only motivated if the transition matrix element is dominated by contributions from very large r. This is the case for reactions at very small energies; while for real experimental energies ($E \gtrsim 100$ keV), the WF of the bound state should be constructed in a more realistic way. Our idea is therefore to introduce a model function that describes the bound state $(c+x)$ WF accurately for all distances. This can be achieved by considering the behavior at small and large r. We have already pointed out that the WF should be described by a Whittaker function at large r. Furthermore, the expected $r \to 0$ behavior for a two-body system consisting of pointlike particles is r^{l_0+1}. Both asymptotics are fulfilled using the following model function:

$$\phi_{\tilde{\gamma}}^{\text{"exact"}}(0,r) = \frac{1}{\sqrt{N_{\tilde{\gamma}}}} W_{-\eta_0, l_0+1/2}(2\kappa_0 r)(1-e^{-\kappa_1 r})^{2l_0+1},$$
$$(11)$$

where $N_{\tilde{\gamma}}$ is the normalization constant and $\tilde{\gamma}$ denotes the parameters $\{\kappa_0, \kappa_1, \eta_0\}$. The parameters κ_0 and η_0 are defined by the binding energy, charges, and masses, while κ_1 can be fitted to give the correct distance between particles c and x (or the correct size of the system). Using this WF, and solving the integral 10 numerically, it is possible to get very good estimates for the electromagnetic reaction cross sections. We should also mention that in the limit $k \to 0$ we are actually able to solve the radial integral 10 analytically, except for the normalization constant $N_{\tilde{\gamma}}$.

However, we are searching for a completely analytical model which will also enable us to incorporate many-body effects. Our model function has to be modified accordingly. First, we note that the asymptotic form of the Whittaker function as $r \to \infty$ is

$$W_{-\eta_0, l_0+1/2}(2\kappa_0 r)$$
$$\sim \frac{e^{-\kappa_0 r}}{(2\kappa_0 r)^{\eta_0}} \left[1 - \frac{(\eta_0-l_0)+(\eta_0^2-l_0^2)}{2\kappa_0 r} + \mathcal{O}\left(\frac{1}{r^2}\right) \right].$$
$$(12)$$

Second, for two-body systems in which the clusters have an internal structure, the centrifugal barrier is effectively larger and the WF should behave as r^n (where $n > l_0+1$) as $r \to 0$.

Motivated by this, we put forward the following model function:

$$\phi_\gamma(0,r) = \frac{1}{\sqrt{N_\gamma}} \frac{e^{-\kappa_0 r}}{r^{\eta_0'}} (1-e^{-\kappa_1 r})^p, \quad (13)$$

with norm

$$N_\gamma = \sum_{m=0}^{2p} \binom{2p}{m} (-1)^m (2\kappa_0 + m\kappa_1)^{2\eta_0'-1} \Gamma(1-2\eta_0'),$$
$$(14)$$

where γ denotes the parameters $\{\kappa_0, \kappa_1, \eta_0', p\}$, and p is an integer fulfilling $p > \eta_0' + 1$. The parameter κ_0 is defined by the binding energy and effective mass. By putting $\eta_0' = \eta_0$ we would ensure to reproduce the tail of the WF at very large r. However, the difference between an exact Whittaker function and its asymptotic behavior [first term of Eq. (12)] remains important for $r \lesssim 100$ fm. Therefore, η_0' and κ_1 are used as free parameters in a fit to the "exact" WF (11) in the interval of interest. In this way η_0' will be an *effective* Sommerfeld parameter while κ_1 will still mainly be connected with the size. Note that if $\eta_0 > l_0$, then the second term in Eq. (12) will be negative and consequently we will find that $\eta_0' < \eta_0$. Finally, the integer p is fixed by the small r behavior. For a pure two-body system we will use $p = \langle \eta_0' + l_0 + 1 \rangle$ (where $\langle x \rangle$ is the closest integer to x), while we can take many-body effects into account by putting $p = \langle \eta_0' + n \rangle$.

With this model WF, it is possible to solve the integral (10) exactly as follows:

$$I_{l,\gamma}(k) = \frac{1}{\sqrt{N_\gamma}} \sum_{m=0}^p \binom{p}{m} (-1)^m (m\kappa_1 + \kappa_0 + ik)^{-(l+2+\lambda-\eta_0')}$$
$$\times \Gamma(l+2+\lambda-\eta_0') {}_2F_1\left(l+2+\lambda-\eta_0'; l+1 \right.$$
$$\left. -i\eta(k); 2l+2; \frac{2ik}{m\kappa_1+\kappa_0+ik} \right). \quad (15)$$

Many-body nuclear structure can further be taken into account by considering the possibility that the bound state WF contains several different two-body components

$$\phi(0,r) = \sum_i a_i \phi_{\gamma_i}(0,r), \tag{16}$$

which can be seen as two-body projections of the many-body WF. Note that pure many-body components will not contribute to two-body breakup and, as a result, we will have $\Sigma_i a_i^2 < 1$. Note also that the threshold for two-body breakup will be higher for components where one (or both) of the clusters is excited. Therefore, we define the continuum strength function separately for each component. Finally, we arrive at an analytical formula for the strength function of component i,

$$\left. \frac{dB(E\lambda)}{dE} \right|_i = \frac{e^2 Z^2(\lambda)\mu_{cx}}{\hbar^2} \frac{2\lambda+1}{2\pi^2} \sum_l a_i^2 k^{2l+1} C_l^2(k)$$

$$\times \langle l_0 0 \lambda 0 | l 0 \rangle^2 |I_{l,\gamma_i}(k)|^2. \tag{17}$$

B. One-neutron halo systems

The special case where $Z_x = 0$, i.e., a one-neutron halo system will lead to several simplifications. First of all we will have $\eta_0 = 0$ and the Whittaker function in Eq. (11) will transform into a modified, spherical Bessel function

$$W_{0,l_0+1/2}(2\kappa_0 r) = \sqrt{\frac{2\kappa_0 r}{\pi}} K_{l_0+1/2}(\kappa_0 r). \tag{18}$$

Furthermore, the continuum solution will reduce from a Coulomb function (7) to the corresponding component of a plane wave

$$\phi_l^{(1n)}(k,r) = \sqrt{\frac{2}{\pi}} i^l r j_l(kr), \tag{19}$$

where $j_l(x)$ is a spherical Bessel function. In this case, the integral (10) can be solved exactly. Consider, e.g., a nodeless s state, for which our model WF would read

$$\phi_{\tilde{\gamma}}^{(1n,1s)}(0,r) = \frac{1}{\sqrt{N_{\tilde{\gamma}}^{(1n,s)}}} e^{-\kappa_0 r}(1 - e^{-\kappa_1 r}), \tag{20}$$

with norm

$$N_{\tilde{\gamma}}^{(1n,1s)} = \frac{\kappa_1^2}{2\kappa_0(\kappa_1 + 2\kappa_0)(\kappa_1 + \kappa_0)}. \tag{21}$$

The radial integral (10) for this special case will be given by

TABLE I. Parameters of our model WFs used to describe the ^{8}B ground state. Both models give the same intercluster distance, $r_{rms} = 4.57$ fm. With $E_0 = 137$ keV we get $\kappa_0 = 0.076$ fm^{-1} and $\eta_0 = 1.595$. The excited core component (last row) has $E_0 = 566$ keV giving $\kappa_0 = 0.154$ fm^{-1} and $\eta_0 = 0.786$. The relative orbital momentum for all components is $l_0 = 1$ while I is the channel spin and a^2 is the spectroscopic factor. Note that there is no dependence on the particular value of the channel spin in the two-body case.

Model WF	configuration	I	a^2	p	κ_1 (fm^{-1})	η_0'/η_0
Two-body	$[^7\text{Be}(3/2^-)\otimes p]$	2	1.00	3	0.601	0.79
Three-body	$[^7\text{Be}(3/2^-)\otimes p]$	2	0.65	5	0.702	0.87
	$[^7\text{Be}(3/2^-)\otimes p]$	1	0.13	5	0.765	0.86
	$[^7\text{Be}(1/2^-)\otimes p]$	1	0.16	5	0.753	1.43

$$I_{l,\tilde{\gamma}}^{(1n,1s)}(k) = \frac{1}{\sqrt{N_{\tilde{\gamma}}^{(1n,1s)}}} \frac{(2l)!!(l+1+\lambda)!}{2^l l!}$$

$$\times \sum_{m=0}^{1} (-1)^m (m\kappa_1 + \kappa_0)^{-(l+2+\lambda)} {}_2F_1$$

$$\times \left(\frac{l+2+\lambda}{2}; \frac{l+3+\lambda}{2}; \frac{3}{2}+l; \frac{-k^2}{(m\kappa_1+\kappa_0)^2} \right). \tag{22}$$

C. Application to ^{8}B

We will now apply our model to the ^{8}B nucleus. The low-lying ^{8}B continuum can, with relatively good precision, be approximated as a pure Coulomb one. At least there are no negative parity states at low excitation energies [25–27] and the electromagnetic processes are, in all cases we are considering, dominated by $E1$ transitions. However, we will also show that the influence of a broad negative parity state at high excitation energy [26,27] is not negligible at intermediate ($\gtrsim 0.4$ MeV) continuum energies.

In a first approximation the bound state of ^{8}B can be treated as a pure two-body (^{7}Be+p) system with binding energy $E_0 = 137$ keV and relative orbital momentum $l_0 = 1$. The single free parameter κ_1 in our "exact" model function (11) was then fitted to an rms intercluster distance of $r_{rms} = 4.57$ fm (extracted from Ref. [28]). In order to get analytical results, we then introduced the model function (13). We put $p = 3$ and fixed κ_0 from the binding energy, while the remaining parameters κ_1 and η_0' were fitted to the behavior of the "exact" model WF, see Table I. The resulting $E1$ strength function is shown as a dotted line in Fig. 1. This analytical approximation agrees very well with numerical results obtained keeping the "exact" model WF. The error is less than 2% in the region of interest.

However, concerning the structure of the ^{8}B ground state one should keep in mind that the ^{7}Be core is in itself a weakly bound system with an excited $1/2^-$ state at 429 keV. The common treatment of ^{8}B as a pure two-body system is therefore questionable. We want to investigate what effect
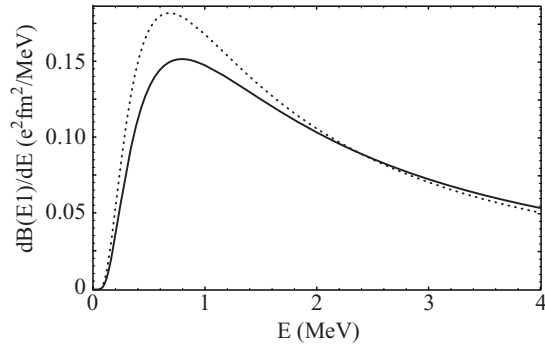
FIG. 1. The $E1$ strength function of ^{8}B. Although the total strengths are the same in these examples, the shapes are very different when treating the ^{8}B nucleus as a two-body (dotted line) or a three-body (solid line) system. The difference is mainly due to the stronger centrifugal barrier in the three-body case (see, e.g., Ref. [29]), which forces the WF to be narrower in coordinate space and thus wider in momentum/energy space. The parameters of the model WFs can be found in Table I.

the many-body structure of ^{8}B might have on the strength function. For this purpose we utilize a recent three-body ($\alpha + {}^3\text{He} + p$) calculation [28] where it was shown that, after projection onto the two-body channels, there are three main components (adding up to 94% of the total WF, see Table I) and that the rest are pure three-body channels. For each of the numerical two-body overlap functions we fit our parameters κ_1 and η_0'. The binding energy $E_0 = 137$ keV determines κ_0 for the two first components and $E_0 = 566$ keV for the third, ^{7}Be excited state, component. The best fit to the small r behavior is obtained with $p = 5$ which reflects the effectively larger centrifugal barrier in the three-body case. This centrifugal barrier will push the WF away from $r = 0$ and will, thus, force it to become more narrow than the corresponding two-body WF.

D. Studies of the corresponding potential

Using the two-body WF (11), which describes correctly the binding energy and the geometry, we are able to restore the corresponding two-body potential. Besides centrifugal barrier and Coulomb interaction, the potential also contains an attractive part which we find can be approximated with a high accuracy by one or two Yukawa-type potentials. Note that such potentials are widely used in few-body nuclear physics. In Fig. 2, the nuclear part of the potential which corresponds to our ^{8}B "exact" two-body WF is plotted. As is shown in the figure, the potential can be very well described by a Yukawa-type potential. In this connection we would also like to point out that for the special case where $l_0 = 0$ and $Z_x = 0$, the WF can be described by (20) and the corresponding potential reduces to a Hulthén potential which has exact solutions.

IV. ELECTROMAGNETIC DISSOCIATION

The EMD of loosely bound nuclei, impinging on a high-Z target, has been used in nuclear physics for many years both in order to investigate nuclear structure and as an indirect
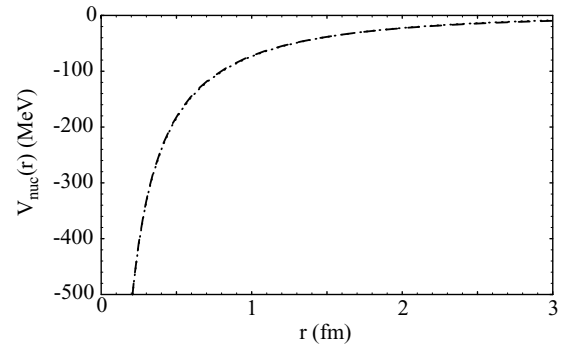

FIG. 2. The nuclear potential (dotted line) corresponding to our ^{8}B "exact" WF. This potential is very well described by a Yukawa potential $V_{\text{nuc}}(r) = -114 e^{-0.457r}/r$ (MeV) (dashed line).

method to extract information on radiative capture reactions. Unfortunately, as for all reaction experiments, a lot of information is contained in the experimental results and it is a hard task to disentangle the desired part. The transition matrix elements represent the probability for an initial state wave function to end up in a specific final state after being filtered through the reaction mechanism. Naturally, both the structure of the initial as well as the final state are important for this quantity. In addition, further complications arise if nuclear induced breakup contributes to the measured cross section, and/or if the interaction time is long enough for higher-order transitions to become important. Therefore, in order to minimize interference from higher-order dynamical effects and from nuclear interactions, we will be interested in high-energy experiments in which events characterized by large impact parameters have been selected.

In this section we will demonstrate that the analysis of EMD energy spectra from loosely bound nuclei is highly model dependent. We will then discuss the important issue of how to separate the contributions from specific multipoles; a problem which is of great significance when extracting information on the inverse, radiative capture reaction.

A. Model dependence of energy spectrum analysis

Applying our analytical model to study EMD using first-order perturbation theory enables us to investigate the sensitivity of the energy spectrum to some properties of the initial bound state. At small relative energies the electromagnetic processes are highly peripheral, which means that the interaction mainly probes the external part of the bound state WF. As a consequence, the amplitude of the EMD cross section should depend crucially on the size of the nuclear system. A larger size implies a lower Coulomb barrier, which results in a larger tunneling probability, and consequently a larger cross section. However, the radii of nuclei far from stability are usually extracted from interaction cross section measurements, and this procedure has unfortunately proven to be highly model dependent. A Glauber-type analysis, assuming a uniform density distribution, results in a smaller radius as compared to an analysis in which the few-body structure is taken into account explicitly [30]. Furthermore, the relevant parameter for two-body breakup is in reality the intercluster
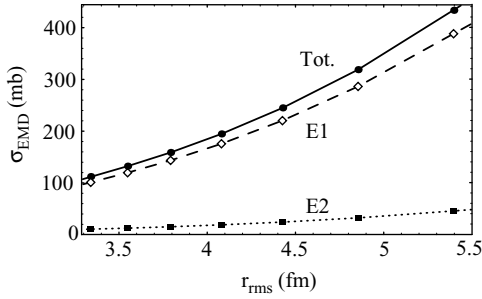
FIG. 3. The total EMD cross section as a function of intercluster distance. The parameter κ_1 of our two-body model WF was varied in order to change the rms distance between the ^{7}Be core and the valence proton. A beam energy of 82.7 MeV/nucleon and a minimum impact parameter of 30 fm was used.

distance rather than the total matter radius, and the relation between these two quantities is also model dependent. In a pure two-body model one often assumes that the size of the core is equal to the size of the corresponding free nucleus. In contrast, taking many-body structure into account will result in polarization effects. For example, it was found in Ref. [31] that the average distance between ^{3}He$-\alpha$ is approximately 10% smaller inside ^{8}B (studied in a ^{3}He$+\alpha+p$ picture) than in a free ^{7}Be nucleus (^{3}He$+\alpha$ picture).

We have investigated the sensitivity of the EMD cross section to the rms intercluster distance by performing model calculations with a ^{8}B-like system. A pure two-body system with $l_0=1$ relative motion (having unity spectroscopic factor) was assumed and a binding energy of 0.137 MeV was used. The effective Sommerfeld parameter was fitted to the asymptotic behavior of Eq. (11), i.e., to the Whittaker tail. The size of our model WF (13) was then a function of the remaining free parameter κ_1. By varying this parameter we could investigate the sensitivity to the size and from Fig. 3 it is clear how strong it is. Just for illustration: a 15% uncertainty in the rms intercluster distance (which, in our model, would correspond to 5% uncertainty in the ^{8}B matter radius) results in $\sim$50% ambiguity of the calculated total cross section.

Let us now consider the difference between a two-body and a three-body approach. As was mentioned in Sec. III C, the effectively larger centrifugal barrier in a three-body system will push the relative motion WF away from $r=0$ and consequently force it to become more narrow than the corresponding two-body WF for a given radius. We therefore expect the distribution in momentum/energy space to be broader. This effect is clearly seen in Fig. 1 where the ^{8}B $E1$ strength functions, obtained using our three-body[1] and two-body analytical model WFs, are compared. This difference, seen in the strength function, should be even more pronounced in the energy spectrum since it will be magnified by the spectrum of virtual photons.

In Fig. 4 we compare different calculations of ^{8}B EMD

---

[1]Note that this is not strictly a three-body model, but rather the two-body projection of a three-body WF. However, in the following we will consistently refer to it as three-body results.
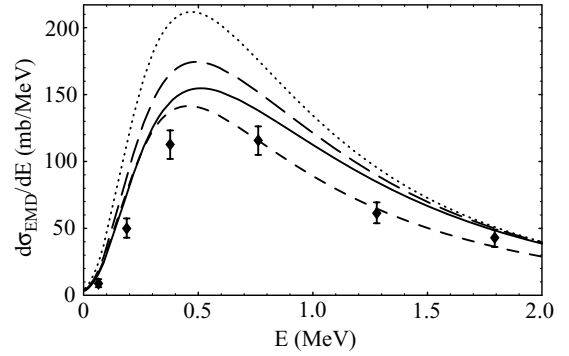

FIG. 4. The ^{8}B EMD energy spectrum obtained at 82.7 MeV/nucleon on Pb with ^{8}B scattering angles $\theta_{8B}\leqslant1.77°$. The data points are from Ref. [3]. The curves show our analytical two-body (dotted line) and three-body (solid line) results, and the numerical calculations: without the FSI (long dashed), and with the FSI (short dashed). All theoretical curves have been corrected for experimental resolution and acceptance.

on Pb, including both $E1$ and $E2$ transitions, to the experimental data from Davids *et al.* [3]. This experiment is very appealing since the selection of scattering angles ($\theta_{8B}\leqslant1.77°$, which corresponds to a minimum impact parameter of $b_{min}=30$ fm) minimizes the contribution from nuclear scattering, and the relatively high beam energy (82.7 MeV/nucleon) justifies the use of first-order perturbation theory. Let us first compare our analytical two-body (dotted line) and three-body (solid line) results, see also Ref. [5]. Concerning the shape of the energy spectrum we have an excellent agreement between the experimental data and our results obtained using the three-body model, while the pure two-body calculation gives a too narrow peak. As to the absolute values, the three-body energy spectrum is $\approx$20% above the experimental data. However, the most important lesson from this comparison is that for two different assumptions concerning the nuclear structure, but keeping the rms intercluster distance fixed, we obtain very different shapes of the calculated energy spectra. Thus, one can conclude that the interpretation of energy spectra is highly model dependent. A final remark in connection to this observation is that, in order to interpret experimental data correctly, it is very important to fix the spectroscopic factors of different two-body and many-body components. Therefore, we want to stress the usefulness of experiments where EMD is studied in complete kinematics. Examples of interesting channels in the ^{8}B case is ^{8}B$\rightarrow^7$Be$(1/2^-)+p+\gamma$ and ^{8}B$\rightarrow^3$He$+\alpha+p$. Some progress has already been made in this direction. Recently, ^{7}Be fragments and γ rays were measured in coincidence after breakup on a light target by Cortina-Gil *et al.* [11], which resulted in a clear observation of the excited core component of the WF.

We have also performed numerical calculations, based on first-order perturbation theory, where the numerical ^{8}B bound state WF from Ref. [28] was used. In the first investigation we assumed a pure Coulomb continuum and the results of this calculation are shown as a long-dashed line in Fig. 4. We note that the obtained energy spectrum compares rather well with our analytical three-body model except for a

15% difference in the peak height. Since our analytical model has the correct asymptotic behavior for large r and a three-body behavior at small r, the main difference to the numerical WF should be in the intermediate region, and this is exactly the region which dominates the transition matrix elements for energies corresponding to the peak of the energy spectrum. This fact explains the observed discrepancy.

In our second numerical investigation we studied the influence of $^7\text{Be}+p$ FSI. As previously mentioned, the low-energy continuum of ^8B is dominated by positive parity states [25] which are only relevant for $E2$ ($\sim 10\%$ of the total cross section) and $M1$ transitions. Note that the latter only plays a role in the vicinity of the narrow 1^+ resonance at 0.64 MeV above threshold, and is therefore not included in our calculations. However, the possible existence of a very broad negative parity state at high excitation energy can still have a strong influence on the energy spectrum. Effects of such a state were observed in a recent elastic proton scattering experiment [27] from which the authors made a 2^- spin-parity assignment and, from an R-matrix analysis, they obtained a best fit with the parameters $E=3.5\pm0.5$ MeV and $\Gamma=8\pm4$ MeV. We have included such a broad continuum structure by adding an attractive potential in the s-wave channel. The effects of this are clearly seen in Fig. 4 (short-dashed line): the total cross section is reduced and the continuum strength is redistributed towards smaller energies. We conclude this comparison by stating that a broad negative parity structure in the high-energy continuum has a non-negligible influence on the EMD energy spectrum for energies $\gtrsim 0.4$ MeV and that the parameters of such a state are still to be determined with greater accuracy.

B. Extraction of $E1$ contribution using the low-E energy spectrum

As we have seen in the preceding section, the main model uncertainties in the EMD analysis are the following: the asymptotic normalization constant which depends on (i) the radius in combination with (ii) the spectroscopic factors of different two-body components, (iii) the underlying many-body structure, and finally, (iv) the FSI. Despite the difficulties connected with measuring the cross section at small relative energies, we still suggest to focus on the low-E part of the energy spectrum. In this way one can avoid uncertainties associated with the FSI (unless there are resonances very close to threshold) and with the many-body behavior of the WF at small intercluster distances. The asymptotic normalization constant in combination with the spectroscopic factor will enter as an absolute normalization of the cross section. However, since this normalization affects all multipole transitions equally it is possible to calculate the ratio of two different multipoles with a very good precision.

We have investigated the ratio

$$R_{\text{EMD}}(E) \equiv \frac{d\sigma_{\text{EMD}}(\text{E1})/dE}{d\sigma_{\text{EMD}}(\text{E1}+\text{E2})/dE}, \qquad (23)$$

and found that it is almost model independent at small relative energies. To demonstrate this we will continue to use the
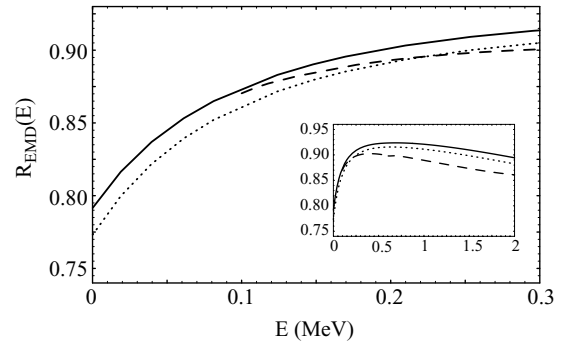

FIG. 5. Fraction of the calculated energy spectrum (EMD of 82.7 MeV/nucleon ^8B on Pb with scattering angles $\theta_{^8\text{B}} \leqslant 1.77°$) attributed to $E1$ transitions, see Eq. (23). The curves show two-body (dotted line) and three-body (solid line) analytical results while the dashed line shows results of numerical calculations including the FSI. The inset shows the same curves for a broader energy range.

EMD of ^8B (on a Pb target at 82.7 MeV/nucleon with b_{min} =30 fm) as an example. Reusing the different model calculations from Sec. IV A, we can investigate the sensitivity of the ratio to different model assumptions. First, in Fig. 5 we can see that the difference between a two-body and a three-body approach is less than 3% in the region of interest. This low sensitivity can be explained by the fact that the low-E part of the spectrum mainly probes the large r asymptotics of the radial WF. Shown in Fig. 5 are also results from the numerical calculations introduced in Sec. IV A. It is clearly seen that the influence from the FSI is almost negligible at small relative energies where the numerical results and our analytical three-body model seem to converge. Unfortunately, the numerical accuracy of our calculations becomes questionable at small energies and the calculated ratio is therefore only plotted down to 0.1 MeV. In this context we want to stress that in our analytical model we are able to calculate the relevant transition matrix elements for all energies, including the limit $E\rightarrow 0$. In contrast, the numerical approaches will run into problems for small energies since the continuum WF will be extremely small at relevant intercluster distances.

Furthermore, as can be seen in Fig. 6, the sensitivity of the $R_{\text{EMD}}(E)$ ratio (23) to the intercluster distance is also very small. This feature is also expected since the intercluster distance determines the asymptotic normalization of the WF which, in turn, cancels when the ratio is calculated. However, as can be seen in the insets of Figs. 5 and 6, the results obtained using the different models diverge with increasing energy.

One final question is well founded: Since the transition matrix elements for very small energies depend mainly on the tail of the bound state WF, is it still justified to use our model WF (13) which has merely an approximate description of the Whittaker tail? The result of our numerical calculation (remember that the numerical bound state WF has the correct asymptotics) presented in Fig. 5 indicates that it is justified, since it seems to converge with the analytical model for small E. Furthermore, in the limit $E\rightarrow 0$ we are actually able to solve the radial integral (10) exactly even for the "exact"
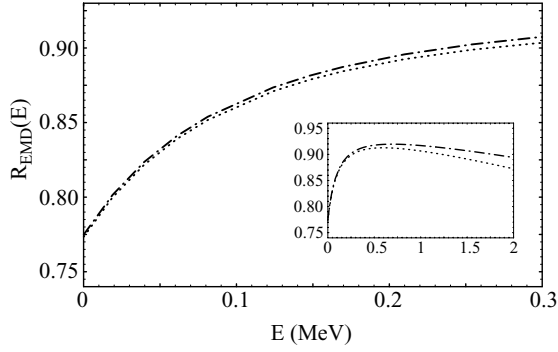
FIG. 6. Fraction of the calculated energy spectrum (EMD of 82.7 MeV/nucleon ^{8}B on Pb with scattering angles $\theta_{^8B} \leqslant 1.77°$) attributed to $E1$ transitions, see Eq. (23). The curves show two-body results characterized by two different intercluster distances: $r_{\text{rms}} = 3.3$ fm (dash dotted) and $r_{\text{rms}} = 5.4$ fm (dotted). The inset shows the same curves for a broader energy range.

WF (11) which has a Whittaker tail. We find that $R_{\text{EMD}}(E \rightarrow 0)$ calculated with the model WF and with the "exact" WF agree within 0.5%. This result gives an additional justification to the use of our model WF for calculating transition matrix elements at small E.

In summary we have found that the calculated $R_{\text{EMD}}(E)$ ratio of the energy spectrum is almost model independent at small relative energies. In the first-order perturbation theory, this ratio can be expressed as

$$R_{\text{EMD}}(E) \equiv \frac{d\sigma_{\text{EMD}}(E1)/dE}{d\sigma_{\text{EMD}}(E1+E2)/dE}$$

$$= 1 \left/ \left(1 + \frac{n_{E2}(E_\gamma)}{n_{E1}(E_\gamma)} \frac{\sigma_\gamma^{E2}(E)}{\sigma_\gamma^{E1}(E)} \right) \right.$$

$$= 1 \left/ \left(1 + \frac{n_{E2}(E_\gamma)}{n_{E1}(E_\gamma)} r_\gamma(E) \right), \right. \quad (24)$$

where we have introduced the $E2/E1$ ratio of photodissociation cross sections

$$r_\gamma(E) \equiv \frac{\sigma_\gamma^{E2}(E)}{\sigma_\gamma^{E1}(E)}. \quad (25)$$

Naturally, the ratio $R_{\text{EMD}}(E)$ will depend on the experimental conditions such as beam energy and minimum impact parameter. However, this dependence enters only in the spectra of virtual photons which are easily calculated for any experimental conditions $\{b_{\min}, E_{\text{beam}}\}$ (see, e.g., Eq. (4.7) of Ref. [23]). In contrast, the ratio of ^{8}B photodissociation cross sections $r_\gamma(E)$ (25) does not depend on the experimental conditions. Therefore, we provide this ratio, calculated within our analytical three-body model, in Fig. 7. The curve shown in Fig. 7 can approximately be described by the formula
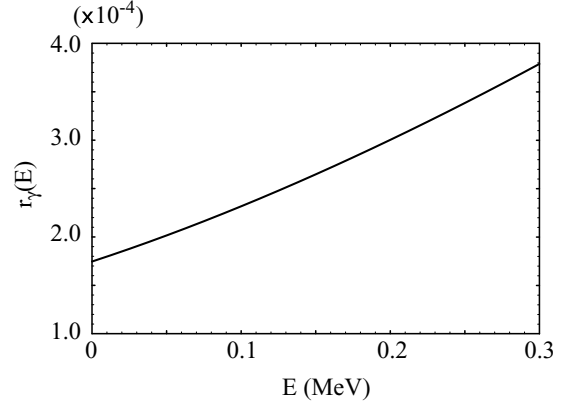

FIG. 7. Ratio of photodissociation cross sections calculated within our analytical three-body model, see Eq. (25).

$$r_\gamma(E) = \frac{\sigma_\gamma^{E2}(E)}{\sigma_\gamma^{E1}(E)} = (-1.7290 + 3.4663 e^{1.5526E}) \times 10^{-4},$$

$$(26)$$

which describes the calculated curve with an accuracy of $<0.5\%$ in the region $0<E<0.3$ MeV. From this formula it is easy to obtain $R_{\text{EMD}}(E)$ using Eq. (24).

C. Extraction of $E1$ contribution using two different experimental conditions

One of the beauties with the method of virtual photons is the separation of reaction kinematics and nuclear excitation dynamics into the spectrum of virtual photons and the photoabsorption cross section, respectively. This separation can be used as an alternative method to extract the $E1$ contribution from the measured cross section. The objective is to use the fact that the cross section will depend on beam energy and minimum impact parameter only through the spectra of virtual photons. First, let us introduce the notation

$$N_{E\lambda}(E_\gamma) = \frac{n_{E\lambda}(E_\gamma, b_{\min}, E_{\text{beam}})}{E_\gamma}, \quad (27)$$

where we have indicated that the spectra of virtual photons are functions of the beam energy and minimum impact parameter. In reality this dependence enters in the adiabaticity parameter

$$\xi = \frac{\omega b_{\min}}{\gamma v}. \quad (28)$$

Assuming that the total cross section is dominated by $E1$ and $E2$ transitions we find that the energy spectrum for given experimental conditions $\{b_{\min}^{(i)}, E_{\text{beam}}^{(i)}\}$ is given by

$$\frac{d\sigma_{\text{EMD}}^{(i)}}{dE} = N_{E1}^{(i)}(E_\gamma) \sigma_\gamma^{E1}(E) + N_{E2}^{(i)}(E_\gamma) \sigma_\gamma^{E2}(E), \quad (29)$$

where we would like to remind the reader of the relation $E = E_\gamma - E_0$. Now we can use the fact that the virtual photon spectra depend differently on ξ for different multipoles to

extract the contribution from one of the multipoles. Let us assume that we have two sets of experimental data from the same experimental setup; the only difference being the beam energy and/or the selected scattering angles (minimum impact parameter). The $E1$ contribution to one of the measurements can then be obtained with the formula

$$
\frac{d\sigma_{\mathrm{EMD}}^{(1)}(E1)}{dE} = \frac{N_{E1}^{(1)}(E_\gamma)}{N_{E1}^{(1)}(E_\gamma)N_{E2}^{(2)}(E_\gamma) - N_{E1}^{(2)}(E_\gamma)N_{E2}^{(1)}(E_\gamma)}
$$
$$
\times \left(N_{E2}^{(2)}(E_\gamma)\frac{d\sigma_{\mathrm{EMD}}^{(1)}}{dE} - N_{E2}^{(1)}(E_\gamma)\frac{d\sigma_{\mathrm{EMD}}^{(2)}}{dE} \right).
$$
(30)

The advantage of this method is that information can be obtained directly from experimental data. However, it should be emphasized that the formula is only valid under the assumptions of the first-order perturbation theory and straight-line trajectories. Thus, this method can only be used for EMD at relatively large beam energies where events characterized by large impact parameters have to be selected. Furthermore, the experimental conditions must be chosen so that the difference $d\sigma_{\mathrm{EMD}}^{(1)}/dE - d\sigma_{\mathrm{EMD}}^{(2)}/dE$ is observable and larger than the experimental uncertainty.

V. CONCLUSION

In this paper, we have studied electromagnetic processes involving loosely bound nuclei. To this aim we have developed an analytical model which is based on the use of radial model functions that give a realistic description of two-body WFs (or the two-body projections of many-body WFs) for all radii, see also Ref. [5]. We have used this model to study EMD of ^{8}B, but have also indicated how it can be applied to other reactions and other nuclei. For example, it should provide an important tool to investigate the low-energy behavior of the astrophysical S factor.

We have also presented numerical calculations based on the three-body model of ^{8}B, developed in Ref. [28], and on recent experimental information on a broad negative parity state in the ^{8}B continuum. Combining the results of our analytical model, and of these numerical calculations, has allowed us to investigate the sensitivity of calculated EMD energy spectra to different model assumptions. We concluded that the magnitude of the cross section depends strongly on the intercluster distance and on the spectroscopic factors of

different many-body channels; while the shape of the energy spectrum is very sensitive to the few-body structure. Finally, we found that a broad negative parity state at high excitation energy will influence the energy spectrum for energies $\gtrsim 0.4$ MeV, and will lead to a reduction of the cross section.

However, the main purpose of this paper has been to investigate the problem of how to extract the $E1$ contribution from a measured EMD energy spectrum. This question is of great significance for the gathering of information on astrophysically interesting radiative capture reactions from EMD experiments [note the relation between the $E1$ component of the EMD energy spectrum and the astrophysical S factor via Eqs. (4)–(6)]. The main method so far has been to study the asymmetries in angular or momentum distributions. However, this asymmetry (which is due to $E1$-$E2$ interference) depends strongly on details of the FSI which, in turn, are often relatively unknown. Furthermore, the $E1$-$E2$ interference terms do not themselves contribute to the integrated cross sections to which the S factor is related. Instead, we have proposed two novel, and less model dependent, approaches to extract the $E1$ contribution from a measured EMD energy spectrum.

(i) First, we demonstrated that the ratio of EMD cross sections $\sigma_{\mathrm{EMD}}(E1)/\sigma_{\mathrm{EMD}}(E1+E2)$ is almost model independent at small relative energies. We also provided an analytical formula to calculate this ratio for any experimental conditions. (ii) Second, we demonstrated how two sets of experimental data, obtained with different E_{beam} and/or b_{min}, can be used to extract the $E1$ component. This method relies on the fact that the strengths of different multipole components depend on the beam energy and minimum impact parameter, and in first-order perturbation theory this dependence enters only in the virtual photon spectra.

Since the proposed two methods are not directly connected to each other, they can be used independently and the results can be compared to each other. However, both methods, but in particular the first one, require that the energy spectrum is measured down to very small relative energies (100–300 keV), which will probably prove to be a difficult challenge.

---

[1] G. Baur and H. Rebel, Annu. Rev. Nucl. Part. Sci. **46**, 321 (1996).

[2] H. Esbensen and G.F. Bertsch, Phys. Lett. B **359**, 13 (1995).

[3] B. Davids, S.M. Austin, D. Bazin, H. Esbensen, B.M. Sherrill, I.J. Thompson, and J.A. Tostevin, Phys. Rev. C **63**, 065806 (2001).

[4] H. Esbensen and G.F. Bertsch, Nucl. Phys. **A600**, 37 (1996).

[5] C. Forssén, N. Shul'gina, and M.V. Zhukov, Phys. Lett. B **549**, 79 (2002).

[6] C.A. Bertulani and G. Baur, Nucl. Phys. **A480**, 615 (1988).

[7] T. Otsuka, M. Ishihara, N. Fukunishi, T. Nakamura, and M. Yokoyama, Phys. Rev. C **49**, R2289 (1994).

[8] A. Pushkin, B. Jonson, and M.V. Zhukov, J. Phys. G **22**, 95 (1996).

[9] C. Forssén, V.D. Efros, and M.V. Zhukov, Nucl. Phys. **A697**, 639 (2002).

[10] C. Forssén, V.D. Efros, and M.V. Zhukov, Nucl. Phys. **A706**, 48 (2002).

[11] D. Cortina-Gil *et al.*, Phys. Lett. B **529**, 36 (2002).

[12] N. Iwasa *et al.*, Phys. Rev. Lett. **83**, 2910 (1999).

[13] T. Kikuchi *et al.*, Phys. Lett. B **391**, 261 (1997).

[14] F. Hammache *et al.*, Phys. Rev. Lett. **86**, 3985 (2001).

[15] R.F. Christy and I. Duck, Nucl. Phys. **24**, 89 (1961).

[16] H.M. Xu, C.A. Gagliardi, R.E. Tribble, A.M. Mukhamedzhanov, and N.K. Timofeyuk, Phys. Rev. Lett. **73**, 2027 (1994).

[17] A. Csótó and K. Langanke, Nucl. Phys. **A636**, 240 (1998).

[18] B.K. Jennings, S. Karataglidis, and T.D. Shoppa, Phys. Rev. C **58**, 3711 (1998).

[19] F.C. Barker and A.M. Mukhamedzhanov, Nucl. Phys. **A673**, 526 (2000).

[20] D. Baye, Phys. Rev. C **62**, 065803 (2000).

[21] A.M. Mukhamedzhanov and F.M. Nunes, Nucl. Phys. **A708**, 437 (2002).

[22] A. Winther and K. Alder, Nucl. Phys. **A319**, 518 (1979).

[23] C.A. Bertulani and G. Baur, Nucl. Phys. **A442**, 739 (1985).

[24] *Handbook of Mathematical Functions*, edited by M. Abramowitz and I. A. Stegun (Dover, New York, 1972).

[25] F. Ajzenberg-Selove, Nucl. Phys. **A490**, 1 (1988).

[26] V.Z. Gol'dberg, G.V. Rogatchev, V.I. Dukhanov, I.N. Serikov, and V.A. Timofeev, Pis'ma Zh. Eksp. Teor. Fiz. **67**, 959 (1998) [JETP Lett. **67**, 1013 (1998)].

[27] G.V. Rogachev *et al.*, Phys. Rev. C **64**, 061601(R) (2001).

[28] L.V. Grigorenko, B.V. Danilin, V.D. Efros, N.B. Shulgina, and M.V. Zhukov, Phys. Rev. C **60**, 044312 (1999).

[29] L.M. Delves, Nucl. Phys. **20**, 275 (1960).

[30] J.S. Al-Khalili and J.A. Tostevin, Phys. Rev. Lett. **76**, 3903 (1996).

[31] L.V. Grigorenko, B.V. Danilin, V.D. Efros, N.B. Shulgina, and M.V. Zhukov, Phys. Rev. C **57**, R2099 (1998).